nature neuroscience

Technical Report

https://doi.org/10.1038/s41593-024-01595-6

Real-time analysis of large-scale neuronal imaging enables closed-loop investigation of neural dynamics

Received: 25 August 2022

Accepted: 7 February 2024

Published online: 11 March 2024

Check for updates

Chun-Feng Shang[1,2,3,8], Yu-Fan Wang[1,4,8], Mei-Ting Zhao[5,6,8], Qiu-Xiang Fan[5,6], Shan Zhao[1,4], Yu Qian[1], Sheng-Jin Xu[1,4], Yu Mu[1,4] ✉, Jie Hao[4,5,6] ✉ & Jiu-Lin Du[1,4,7] ✉

Large-scale imaging of neuronal activities is crucial for understanding brain functions. However, it is challenging to analyze large-scale imaging data in real time, preventing closed-loop investigation of neural circuitry. Here we develop a real-time analysis system with a field programmable gate array–graphics processing unit design for an up to 500-megabyte-per-second image stream. Adapted to whole-brain imaging of awake larval zebrafish, the system timely extracts activity from up to 100,000 neurons and enables closed-loop perturbations of neural dynamics.

Understanding the brain function relies on complete measurement and closed-loop perturbation of neural dynamics[1,2]. Advanced optical imaging realizes measurement of neural dynamics across large populations of neurons[3–7]—even at the whole-brain scale in small vertebrate animals such as zebrafish[5,8–10]. For closed-loop perturbation, real-time analysis is a prerequisite for capturing the moment when the target neural dynamics emerge[1,2,11–14]. Although real-time analysis has been achieved for relatively small-scale optical imaging[15,16], it is still unfeasible for large-scale imaging due to exponentially increased data stream rate. Therefore, existing techniques are insufficient for the implementation of closed-loop experimental paradigms important for causal investigation of large-scale neural dynamics[1,2]. Here we developed a real-time system for analyzing large-scale imaging data and applied it to whole-brain imaging of awake larval zebrafish. With a customized field programmable gate array–graphics processing unit (FPGA-GPU) system, we could analyze the brain-wide neural dynamics during acquisition and deliver optogenetic and sensory stimuli upon the occurrence of the target neural dynamics. Such a closed-loop strategy was exemplified by showing optogenetic manipulation and visual processing regulation locked to specific brain states, and a virtual reality (VR) directly driven by brain-wide neuronal activities.

Results

In real-time analysis of optical imaging, the main challenge is to speed up two processes: the assembling of images from the camera data stream and the massive structured computations in image registration. Similar requirements were met in astronomy studies. For example, in the real-time detection of fast radio bursts[17], an analysis pipeline has been developed based on an FX design[18]. We employed the FX design, in which a customized field programmable gate array (FPGA) board and two graphics processing units (GPUs) work in series, to extract targeted neural dynamics from whole-brain imaging of awake larval zebrafish (Fig. 1a and Extended Data Fig. 1). The FPGA board acquires the data stream of the image sensor, a scientific CMOS camera (sCMOS; Orca Flash 4.0, Hamamatsu), assembles image frames from the data stream and feeds them to two GPUs via 10 gigabit ethernet ports (Extended Data Fig. 2). The two GPUs (P100, NVIDIA) are utilized to perform simultaneous registration of every two adjacent frames, correcting the drifting and distortion and minimizing possible artifact signals. The registration algorithm employed in our system is a piecewise rigid registration algorithm that has been developed and introduced for whole-brain imaging of zebrafish[8,19]. Neuronal activities are then extracted from predefined regions of interest (ROIs). Finally, single-neuron activities are pooled

[1]Institute of Neuroscience, State Key Laboratory of Neuroscience, Center for Excellence in Brain Science and Intelligence Technology, Chinese Academy of Sciences, Shanghai, China. [2]Guangdong-Hongkong-Macau Institute of CNS Regeneration, Ministry of Education CNS Regeneration Collaborative Joint Laboratory, Jinan University, Guangzhou, China. [3]Shenzhen Institute of Neuroscience, Shenzhen, China. [4]University of Chinese Academy of Sciences, Beijing, China. [5]Institute of Automation, Chinese Academy of Sciences, Beijing, China. [6]Guangdong Institute of Artificial Intelligence and Advanced Computing, Guangzhou, China. [7]School of Life Science and Technology, ShanghaiTech University, Shanghai, China. [8]These authors contributed equally: Chun-Feng Shang, Yu-Fan Wang, Mei-Ting Zhao. ✉e-mail: my@ion.ac.cn; jie.hao@ia.ac.cn; forestdu@ion.ac.cn

https://doi.org/10.1038/s41593-024-01595-6

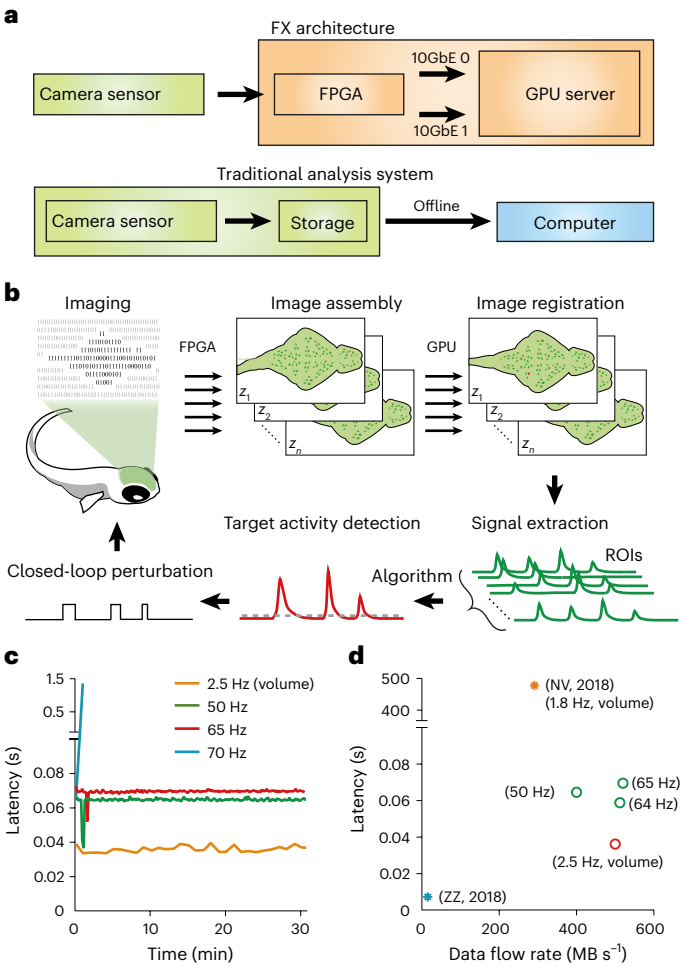

Fig. 1 | Stable real-time analysis of optical imaging of large-scale neuronal activities. a, FX design-based real-time analysis system for large-scale imaging, in comparison with traditional imaging analysis. In the FX design, a customized FPGA board and two GPUs work in series. **b**, Illustration of the whole-brain functional imaging and closed-loop delivery of feedback perturbation enabled by the real-time analysis system. Imaging data stream (binary bits) is assembled into image frames and registered by the customized FPGA-GPU system. Neuronal activities are extracted from predefined ROIs (green traces). The feedback perturbation (black trace) is delivered when the computed neural activity (red trace, computed with a preset algorithm, for example, averaging, interneuronal variance and so on) surpasses a threshold (dashed line). **c**, Stable generation of feedback signals with a latency of <70.5 ms, measured during single-plane imaging at various frame rates (determining data stream rates) or during volumetric imaging at 2.5 Hz (25 frames per volume). **d**, Feedback latency during stable imaging with various data stream rates, compared with previously reported data obtained with volumetric light-sheet microscopy ('(NV, 2018)')[9] or point-scanning two-photon microscopy ('(ZZ, 2018)')[15]. 10GbE, 10 gigabit ethernet.

by a preset algorithm and the calculated population neural dynamics are used to update external stimuli used for closed-loop perturbation (Fig. 1b). The external stimuli were updated with a feedback latency of less than 70.5 ms, which consists of the time spent on the system initiation, data transmission and data processing (Fig. 1c,d and Supplementary Table 1). The total data processing time per frame was measured to be ~15 ms. Therefore, the highest frame rate that supports real-time computation is ~65 Hz (that is 1/0.015 Hz), with the data stream rate up to 520 MB s^{-1} (Fig. 1c,d). As the axial position (layer ID in Extended Data Fig. 1) is appended with each image frame and the GPU computation is easily reconfigurable, the system can adapt to different microscopes and is switchable between single-frame imaging and volumetric imaging. The signals ($\Delta F/F_0$), accessed by calcium-dependent fluorescence change (ΔF) relative to its basal level (F_0), from up to 100,000 ROIs across the whole brain of larval zebrafish can be continuously extracted in the volumetric imaging mode (Fig. 2a–d). In comparison with current state-of-the-art online imaging analysis systems, our system's feedback latency (70.5 ms, primarily determined by the time for real-time image registration and cell response extraction) is much shorter than that of the volumetric light-sheet imaging reported[9] (~480 s with 295 MB s^{-1}, including a data transferring and computer cluster computing time in '(NV, 2018)', Fig. 1d), enabling real-time processing. Furthermore, our data acquisition speed (~500 MB s^{-1}) is 30 times faster than that of the point-scanning methods, including resonant-scanning two-photon fluorescent microscopy[15] (~15 MB s^{-1}, '(ZZ, 2018)' in Fig. 1d), allowing flexible monitoring of activities from neuronal ensembles across the brain.

Neuronal ensembles, characterized by coordinated population activity patterns, are believed to play important roles in perception, decision-making, motor control and other neural processes. Here we monitored the activity of neuronal ensembles by pooling real-time extracted neuronal signals across the brain and performed closed-loop perturbations (Fig. 2 and Extended Data Fig. 3). Neurons were clustered into distinct ensembles and could be individually assigned weights based on experimental requirement. When the weighted average activity of a 'seed cluster' exceeded a predetermined threshold, a trigger signal was generated to initiate optogenetic or sensory stimulation (Fig. 2a–d). For closed-loop optogenetic perturbation, we used the triple-transgenic zebrafish line Tg(HuC:H2B-GCaMP6f);Tg(vglut2a:GAL4FF);Tg1(UAS:ChrimsonR-mKate2);nacre, which expresses the calcium indicator GCaMP6f in all neurons and the optogenetic actuator ChrimsonR in glutamatergic neurons. The ensemble activity of a cluster in the optic tectum ('seed cluster') was then monitored and used to trigger optogenetic stimulation on the ipsilateral tegmentum ('optogenetic target', Fig. 2e–g). This closed-loop stimulation elicited neuronal responses in the tegmentum and other downstream brain regions (Fig. 2g–j).

Brain-wide neural functions, including response to environmental changes, are dynamically modulated by ongoing brain state. The synchronous activation of norepinephrinergic (NE) neurons in the locus coeruleus (LC) tightly correlates with the arousal state and potentiates sensory responsiveness[20,21]. We imaged the neuronal activities across the whole brain and delivered sensory stimuli when LC-NE neurons displayed synchronous activities (Fig. 3a). Using the triple-transgenic zebrafish line Ki(dbh:Gal4-VP16);Tg(HuC:H2B-GCaMP6f);Tg(UAS:mCherry);nacre, in which GCaMP6f is expressed in all neurons and the red fluorescent protein mCherry in NE neurons, the LC-NE neuronal activities were extracted from the whole-brain neuronal dynamics. Spontaneous activities of LC-NE neurons switched between synchronous activation and silence (Extended Data Fig. 4), indicating alternations between different brain states[20,21]. When light flashes were delivered without coupling to LC-NE activation, flash-evoked responses mainly localized in the optic tectum and the thalamus (Fig. 3b), consistent with the previous findings[22]. Interestingly, when sensory stimuli were delivered precisely upon the synchronous activation of LC-NE neurons, the same flash evoked larger responses and recruited more neurons (from 9,907 to 21,357) in broader brain areas, including the cerebellum and the hindbrain (Fig. 3c–g). It is worth noting that a minority of neurons exhibited decreased responses (Fig. 3e), indicating diverse modulatory effects of LC-NE activation on neuronal activities. These results suggest that sensory-evoked response depends on the brain state, and closed-loop stimulus delivery can probe the interaction of the inner state and the external environment more precisely and efficiently.

We next exploited the real-time feedback for a neuronal activity-based brain–computer interface. Whole-brain neuronal activities encapsulate the information required for interacting with

https://doi.org/10.1038/s41593-024-01595-6

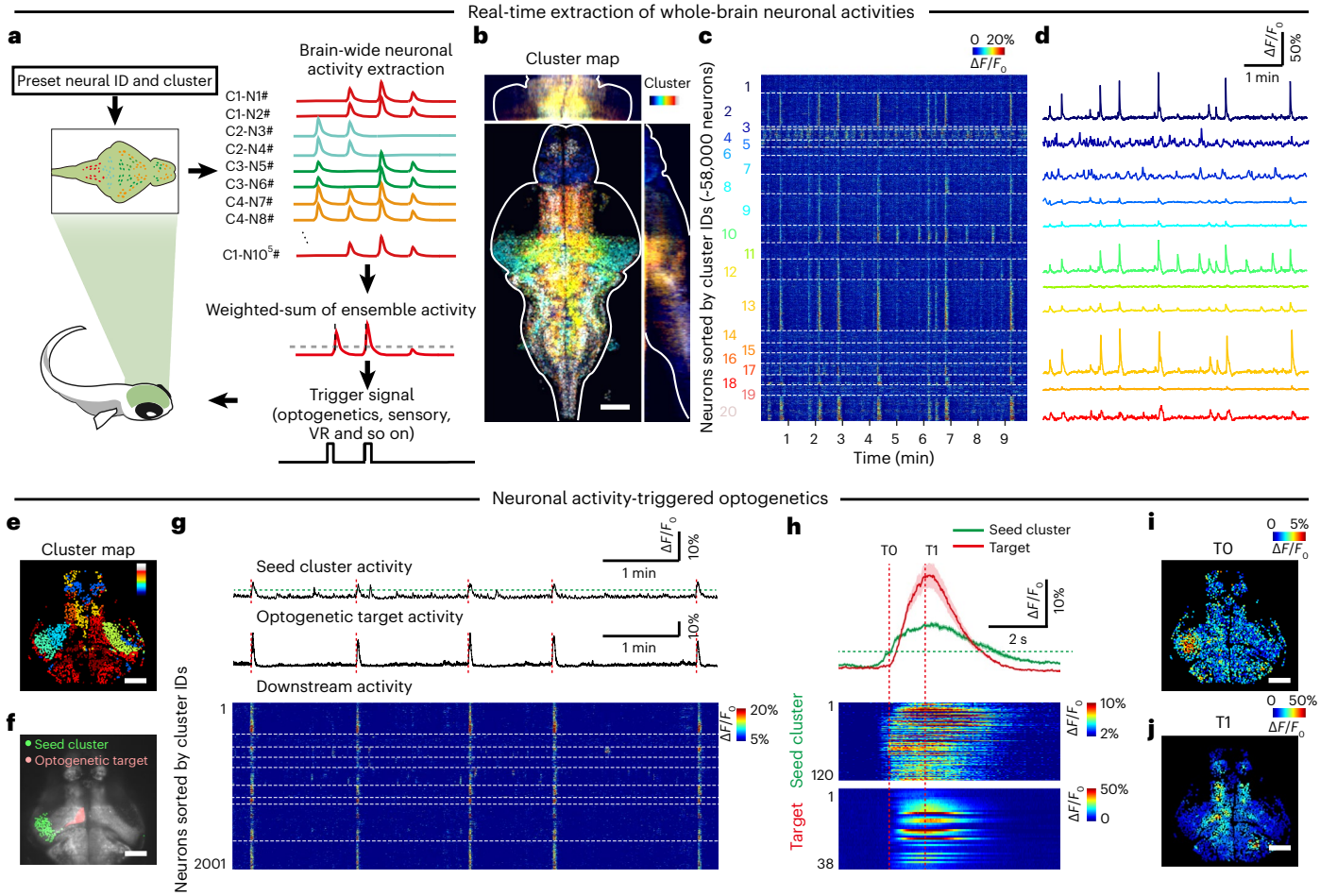

Fig. 2 | Real-time extraction of brain-wide neuronal activities enables ensemble activity-triggered optogenetics. a, Experimental design of ensemble activity-triggered closed-loop perturbations. Brain-wide neuronal activities are extracted in real time and the weighted sum of ensemble activities is used to trigger feedback stimuli, including optogenetics, sensory, VR and so on. Cluster ('C') identities are assigned to each neuron ('N') based on their functional diversities. **b**, Brain-wide neurons are shown for their anatomical positions in the zebrafish brain, with the cluster identity coded by color. Scale bar, 100 µm. **c**, Heatmap displaying spontaneous neuronal activities for approximately 58,000 neurons sorted into 20 clusters across the brain. Neurons are ordered based on their cluster ID. **d**, Weighted average ensemble activity of representative clusters with their IDs coded by color. **e**, Functional clusters derived from spontaneous neuronal activities. The ensemble activity of a seed cluster (cyan) in the left lateral tectum was used for triggering optogenetic stimulation. **f**, Spatial location of both the seed cluster and optogenetic target in the left tegmentum. **g**, Ensemble activity of the seed cluster (top) triggers optogenetic stimulation (red dashed lines) when surpassing a preset triggering threshold (green dashed line). This strongly evoked the activity of the target cluster (middle) and across the brain (heatmap, bottom). Note that a minimum interval of 1 min is required for the nearest stimuli. **h**, Distinct temporal dynamics between the seed and the target cluster are revealed in both trial-averaged ensemble activities (top) and individual neuronal activities (middle and bottom). T0, the frame triggering optogenetic stimulation; T1, the frame at optogenetic stimulation offset. The error bands indicate s.e.m. **i**, Response map at T0. **j**, Response map at T1. Scale bars, 100 µm for **e**,**f**,**i**,**j**. The triple-transgenic zebrafish line Tg(HuC:H2B-GCaMP 6f);Tg(vglut2a:GAL4FF);Tg1(UAS:ChrimsonR-mKate2);nacre was employed and optogenetic stimuli were delivered by using a 589-nm laser.

the environment, and could serve as an ideal source of inputs for a brain–computer interface[11–16]. We transformed a previously established 'motor-controlled' VR paradigm[23–25] into a 'neuron-controlled' version. Under 'motor-control', the locomotor drive (fictive swim recorded from the motor nerves of paralyzed larval zebrafish) is translated to visual feedback; under 'neuron-control', the population activity of a swimming-relevant neuronal ensemble updates the visual feedback in real time (Fig. 3h, Supplementary Video 1 and Extended Data Fig. 5). We compared the efficacy of the 'neuron-control' approach with the 'motor-control' approach. Both the neuronal population activity and the locomotor drive faithfully recreated visual displacements during swimming, according to a feedback gain (Fig. 3i,j). We designed the feedback gain to periodically alternate between a high and a low level to evaluate if the animal could make compensatory changes to adapt to the virtual environment. Both inputs successfully established a closed-loop control (Fig. 3i–l). In the 'motor-control' mode, the animal engaged with the environment by increasing or decreasing the 'fictive swims' during the low- or high-gain conditions, respectively (Fig. 3j,l). Correspondingly, in the 'neuron-control' mode, the real-time population activity from the selected neuronal ensemble showed similar compensatory modulation (Fig. 3i,k) (gain adaptation index: 1.74 ± 0.085 for the 'neuron-control' mode versus 1.70 ± 0.15 for the 'motor-control' mode; $P = 0.15$, Mann–Whitney test). Thus, this real-time analysis system is fast and accurate for extracting neuronal dynamics and generating closed-loop control of the environments in VR.

Discussion

In summary, we introduce an FPGA-GPU-based system for the real-time analysis of near-gigbyte per second optical imaging of neuronal activities. In this system, the data interface modules are flexible and the

https://doi.org/10.1038/s41593-024-01595-6

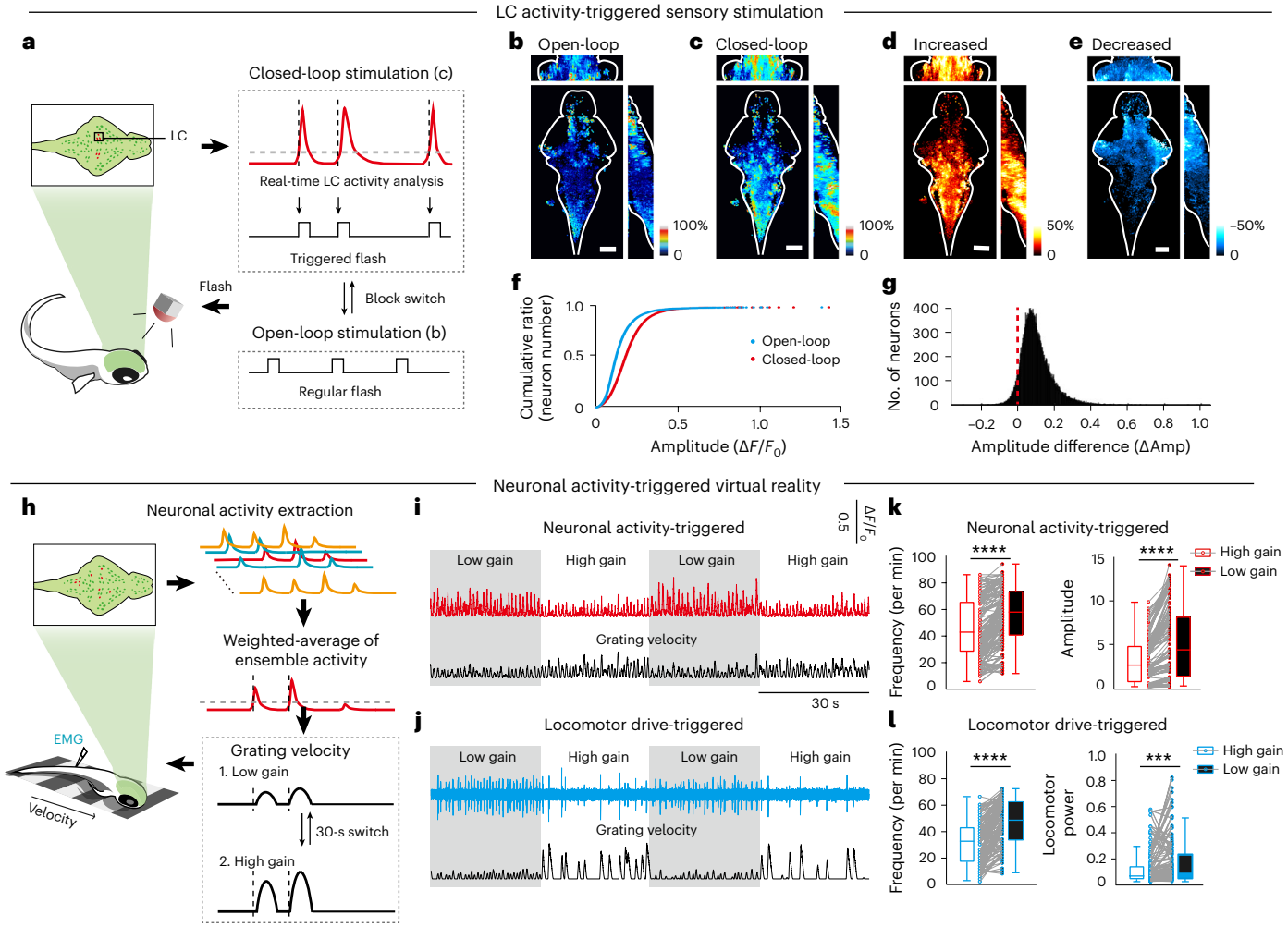

Fig. 3 | Real-time analysis of brain-wide neuronal activities enables experiments of closed-loop sensory stimulation and VR. a, Experimental design of closed-loop sensory stimulation. A light flash (black traces) was delivered during the synchronous activation of LC-NE neurons (red trace). The synchronous activity of LC-NE neurons was computed in real time, compared with a preset threshold (dashed line), and used to trigger light flashes (closed-loop stimulation). In a control experiment, light flashes were applied regardless of LC-NE activities (open-loop stimulation). **b**,**c**, Maps of activated neurons under open-loop (**b**) or closed-loop (**c**) delivery of flash stimulation. **d**,**e**, Map highlighting increased (**d**) and decreased (**e**) responses in the closed-loop mode compared with the open-loop mode. Scale bars, 100 µm for **b**–**e**. **f**, Cumulative amplitude distribution of flash-evoked neuronal responses under open-loop (blue) or closed-loop mode (red). **g**, Closed-loop stimulus-evoked sensory responses in a supralinear manner. For each neuron, its amplitude difference (ΔAmp) is calculated as $\Delta Amp = R_{closed\text{-}loop} - (R_{open\text{-}loop} + R_{LC\text{-}only})$, where a positive value indicates that the neuronal response evoked in the closed-loop mode is greater than the sum of response evoked by open-loop stimuli and the spontaneous activity of the same neuron when the LC-NE system is active. $R_{LC\text{-}only}$, the spontaneous activity from trials with LC-NE activation but without visual stimulation. In the majority of neurons, the flash-evoked activity under closed-loop mode exceeds the summation of the spontaneous activity and the activity evoked in open-loop mode. **h**, Experimental design of a VR enabled by ensemble neuronal activity-triggered sensory feedback. Real-time activities were extracted from brain-wide neurons, and their weighted average was used to generate the ensemble activity of a swimming-related neuron cluster (red). This ensemble activity directly modulated the velocity of grating stimulus (black) according to a feedback gain that alternated between low and high levels. Whole-brain imaging was performed on the transgenic zebrafish Tg(HuC:GCaMP8f) at 5–6 d postfertilization. **i**–**l**, Gain adaptation in closed-loop control measured by neuronal activity (**i**,**k**) or locomotor drive (**j**,**l**). In the low-gain condition, both the frequency and amplitude/power of the neuronal ensemble activities (red) and locomotor drive in motor nerves in the trunk (cyan) were significantly larger compared with the high-gain condition. Example traces (**i**,**j**) and population data (**k**,**l**) are shown. ***$P = 0.0027$; ****$P < 0.0001$; two-sided paired t-test; $n = 148$ trials from 11 fish in **k**, $n = 129$ trials from 9 fish in **l**. In the box plots, the central lines mark the medians, the box limits mark the upper and lower quartiles, and the whiskers mark ±1.5 × interquartile range. Data from each individual trial were marked with filled circles and connected with a line. EMG, motor nerve signals.

data stream bandwidth is extensible, thus it can be easily adapted to other large-scale neural recording setups. With the capacity of high-throughput analysis of ongoing neural dynamics, this system can serve as an excellent interface between large-scale internal dynamics and external perturbations. Besides the closed-loop control of optogenetic and sensory stimulation, the system can also enable other closed-loop perturbations (such as photoconversion) through targeting functional ensembles on specific phases of neural dynamics. By looping and iterating the analyzing–perturbing–reanalyzing process in real time, models can be generated, tested and improved during the experiment[1,2].

Online content

Any methods, additional references, Nature Portfolio reporting summaries, source data, extended data, supplementary information, acknowledgements, peer review information; details of author contributions and competing interests; and statements of data and code availability are available at https://doi.org/10.1038/s41593-024-01595-6.

References

1. Grosenick, L., Marshel, J. H. & Deisseroth, K. Closed-loop and activity-guided optogenetic control. *Neuron* **86**, 106–139 (2015).
2. Chen, Z. S. & Pesaran, B. Improving scalability in systems neuroscience. *Neuron* **109**, 1776–1790 (2021).
3. Cardin, J. A., Crair, M. C. & Higley, M. J. Mesoscopic imaging: shining a wide light on large-scale neural dynamics. *Neuron* **108**, 33–43 (2020).
4. Kim, T. H. & Schnitzer, M. J. Fluorescence imaging of large-scale neural ensemble dynamics. *Cell* **185**, 9–41 (2021).
5. Zhang, Z. et al. Imaging volumetric dynamics at high speed in mouse and zebrafish brain with confocal light field microscopy. *Nat. Biotechnol.* **39**, 74–83 (2021).
6. Ren, C. & Komiyama, T. Characterizing cortex-wide dynamics with wide-field calcium imaging. *J. Neurosci.* **41**, 4160–4168 (2021).
7. Urai, A. E., Doiron, B., Leifer, A. M. & Churchland, A. K. Large-scale neural recordings call for new insights to link brain and behavior. *Nat. Neurosci.* **25**, 11–19 (2022).
8. Ahrens, M. B., Orger, M. B., Robson, D. N., Li, J. M. & Keller, P. J. Whole-brain functional imaging at cellular resolution using light-sheet microscopy. *Nat. Methods* **10**, 413–420 (2013).
9. Vladimirov, N. et al. Light-sheet functional imaging in fictively behaving zebrafish. *Nat. Methods* **15**, 1117–1125 (2018).
10. Cong, L. et al. Rapid whole brain imaging of neural activity in freely behaving larval zebrafish (*Danio rerio*). *eLife* **6**, e28158 (2017).
11. Golub, M. D., Chase, S. M., Batista, A. P. & Yu, B. M. Brain-computer interfaces for dissecting cognitive processes underlying sensorimotor control. *Curr. Opin. Neurobiol.* **37**, 53–58 (2016).
12. Peixoto, D. et al. Decoding and perturbing decision states in real time. *Nature* **591**, 604–609 (2021).
13. Scangos, K. W. et al. Closed-loop neuromodulation in an individual with treatment-resistant depression. *Nat. Med.* **27**, 1696–1700 (2021).
14. Clancy, K. B., Koralek, A. C., Costa, R. M., Feldman, D. E. & Carmena, J. M. Volitional modulation of optically recorded calcium signals during neuroprosthetic learning. *Nat. Neurosci.* **17**, 807–809 (2014).
15. Zhang, Z., Russell, L. E., Packer, A. M., Gauld, O. M. & Häusser, M. Closed-loop all-optical interrogation of neural circuits in vivo. *Nat. Methods* **15**, 1037–1040 (2018).
16. Trautmann, E. M. et al. Dendritic calcium signals in rhesus macaque motor cortex drive an optical brain-computer interface. *Nat. Commun.* **12**, 3689 (2021).
17. CHIME/FRB Collaboration. A bright millisecond-duration radio burst from a Galactic magnetar. *Nature* **587**, 54–58 (2020).
18. Amiri, M. et al. The CHIME Fast Radio Burst Project: system overview. *Astrophys. J.* **863**, 48 (2018).
19. Giovannucci, A. et al. CaImAn: an open source tool for scalable calcium imaging data analysis. *eLife* **8**, e38173 (2019).
20. Sara, S. J. & Bouret, S. Orienting and reorienting: the locus coeruleus mediates cognition through arousal. *Neuron* **76**, 130–141 (2012).
21. Breton-Provencher, V. & Sur, M. Active control of arousal by a locus coeruleus GABAergic circuit. *Nat. Neurosci.* **22**, 218–228 (2019).
22. Dunn, T. W. et al. Neural circuits underlying visually evoked escapes in larval zebrafish. *Neuron* **89**, 613–628 (2016).
23. Portugues, R. & Engert, F. Adaptive locomotor behavior in larval zebrafish. *Front. Syst. Neurosci.* **5**, 72 (2011).
24. Ahrens, N. et al. Brain-wide neuronal dynamics during motor adaptation in zebrafish. *Nature* **485**, 471–477 (2012).
25. Vladimirov, N. et al. Light-sheet functional imaging in fictively behaving zebrafish. *Nat. Methods* **11**, 883–884 (2014).